

# Fourier Phase Analysis of SDSS Galaxies

Chiaki HIKAGE and Takahiko MATSUBARA

*Department of Physics and Astrophysics, Nagoya University, Chikusa, Nagoya 464-8602*  
*hikage@phys.nagoya-u.ac.jp, taka@phys.nagoya-u.ac.jp*

Yasushi SUTO

*Department of Physics, School of Science, The University of Tokyo, Tokyo 113-0033*  
*suto@phys.s.u-tokyo.ac.jp*

Changbom PARK

*Korea Institute for Advanced Study, Dongdaemun-gu, Seoul 207-43, Korea*  
*cbp@kias.re.kr*

Alexander S. SZALAY

*Department of Physics and Astronomy, The Johns Hopkins University, Baltimore, MD 21218, USA*  
*szalay@jhu.edu*  
and

Jon BRINKMANN

*Apache Point Observatory, P.O.Box 59, Sunspot, NM 88349-0059, USA*  
*jb@apo.nmsu.edu*

(Received 2005 June 9; accepted 2005 August 11)

## Abstract

We present a first analysis of the clustering of SDSS galaxies using the distribution function of the sum of Fourier phases. This statistical method was recently proposed by one of the authors as a new probe of the phase correlations of cosmological density fields. Since the Fourier phases are statistically independent of the Fourier amplitudes, the phase statistic plays a complementary role to the conventional two-point statistics of galaxy clustering. In particular, we focus on the distribution functions of the phase sum over three closed wavevectors as a function of the triangle configuration. We find that the observed distribution functions of the phase sum are in good agreement with the lowest-order approximation from perturbation theory. For a direct comparison with observations, we construct mock catalogs from  $N$ -body simulations taking account of the survey geometry, the redshift distortion, and the discreteness due to the limited number of data. Indeed the observed phase correlations for the galaxies in the range of the absolute magnitude,  $-22 < M_r < -18$ , agree well with those for  $\Lambda$ -dominated spatially flat cold dark matter predictions with  $\sigma_8 = 0.9$  evolved from the Gaussian initial condition. This agreement implies that the galaxy biasing is approximately linear in redshift space. Instead, assuming that the galaxy biasing is described by a quadratic deterministic function at  $k < 0.03[2\pi/(h^{-1}\text{Mpc})]$ , we can constrain the ratio of the quadratic biasing parameter,  $b_2$ , to the linear biasing parameter,  $b_1$ , from the difference of phase correlations between observations and mock predictions. We find that the resulting  $b_2/b_1$  is well fitted by  $b_2/b_1 = 0.54(\pm 0.06) - 0.62(\pm 0.08)\sigma_8$  and is almost insensitive to the cosmology and luminosity in those ranges. Indeed,  $b_2/b_1$  is nearly zero when  $\sigma_8 = 0.9$ .

**Key words:** cosmology: large-scale structure of universe — cosmology: observations — methods: statistical

## 1. Introduction

The spatial distribution of galaxies, *Large Scale Structure* (LSS), provides fundamental knowledge about the formation and evolution of the density structure in our universe. A recent measurement of the CMB (Cosmological Microwave Background) anisotropy by WMAP (Wilkinson Microwave Anisotropy Probe) puts a stringent constraint on the primordial density fluctuations, and favors the  $\Lambda$ -dominated spatially flat Cold Dark Matter (LCDM) model with a Gaussian initial condition (Spergel et al. 2003; Komatsu et al. 2003). One of the goals in the analysis of galaxy distribution is to

test cosmological models in an independent and complementary manner to the CMB analysis. Another goal is to understand galaxy clustering, with particular emphasis on galaxy biasing, which is a statistical relation of the clustering between galaxies and the underlying dark matter. Recent wide-field galaxy surveys, such as SDSS (Sloan Digital Sky Survey) and 2dFGRS (Two Degree Field Galaxy Redshift Survey), indeed enable a detailed study of galaxy clustering with unprecedented accuracy.

More conventional statistics for analyzing the galaxy distribution is the two-point correlation function, or the power spectrum in Fourier space. Two-point statistics have been extensively studied for more than 35 years

since the pioneer work by Totsuji and Kihara (1969), and have been applied to various redshift surveys, including SDSS (e.g., Tegmark et al. 2004a; Zehavi et al. 2005 for SDSS galaxies; Yahata et al. 2005 for SDSS quasars). They, however, cannot fully describe the statistical nature of the galaxy distribution, because LSS is highly non-Gaussian due to the nonlinear gravitational evolution and nonlinearity in the galaxy biasing. To characterize the non-Gaussian properties of the galaxy distribution requires higher order statistics beyond two-point statistics. Motivated by this requirement, various statistics have been introduced as complementary tools to two-point statistics for the analysis of galaxy clustering: higher order correlation functions (e.g., Peebles 1980), genus statistics (Gott et al. 1986; Hoyle et al. 2002; Hikage et al. 2002; Park et al. 2005), Minkowski functionals (Mecke et al. 1994; Hikage et al. 2003), minimum spanning trees (Barrow et al. 1985), void statistics (White 1979), and so on. While these statistics capture different parts of non-Gaussian features, they are not completely independent of the two-point statistics.

The Fourier transform,  $\delta_{\mathbf{k}}$ , of a density fluctuation field is separately written in terms of the amplitude and the phase,  $\theta_{\mathbf{k}}$ , as

$$\delta_{\mathbf{k}} = |\delta_{\mathbf{k}}| \exp(i\theta_{\mathbf{k}}). \quad (1)$$

The Gaussian fields have a uniform distribution of the Fourier phases over  $0 \leq \theta_{\mathbf{k}} \leq 2\pi$ . Therefore, characterizing the correlation of phases is expected to be a direct means to explore the non-Gaussian features. Furthermore, Fourier phases are statistically independent information of the power spectrum, which is defined by  $|\delta_{\mathbf{k}}|^2$ . Nevertheless, finding useful statistics of the Fourier phases is not easy, mainly because of the cyclic property of the phase. For example, the one-point phase distribution turns out to be essentially uniform, even in a strongly non-Gaussian field (Suginohara, Suto 1991). For this reason, previous studies of the Fourier phase have been mainly devoted to the evolution of phase shifts in individual modes (Ryden, Gramann 1991; Soda, Suto 1992; Jain, Bertschinger 1998), or the phase differences between the Fourier modes (Scherrer et al. 1991; Coles, Chiang 2000; Chiang 2001; Chiang et al. 2002; Watts, Coles 2003).

Matsubara (2003) recently proposed, as a new measure of phase correlations, the distribution function of the “phase sum”,  $\theta_{\mathbf{k}_1} + \theta_{\mathbf{k}_2} + \dots + \theta_{\mathbf{k}_N}$ , where the corresponding wavevectors satisfy  $\mathbf{k}_1 + \mathbf{k}_2 + \dots + \mathbf{k}_N = \mathbf{0}$ . Although a connection between the higher order statistics and the phase correlations was suggested earlier (Bertschinger 1992; Watts, Coles 2003), he discovered an important analytic relation between the distribution function of the phase sum and the polyspectra using perturbation theory.

A subsequent numerical analysis by Hikage et al. (2004) explained the behavior of the phase-sum distribution with respect to the density structure in real space. When a prominent density peak exists in a given sampling volume, the Fourier phases of various modes are synchronized to have nearly zero values at the position of peak, and thus

the phase sum distributes around zero. On the other hand, when several peaks with comparable heights exist, the synchronization of phases is diluted, and thus the phase-sum distribution becomes almost uniform. The phase-sum distribution is sensitive to the non-Gaussian feature of the density field, especially the relative strength of the most high-density peak to other density peaks. The nonlinear gravitational evolution and the nonlinearity in the galaxy biasing statistically changes the relative strength of density peaks in galaxy distribution, and therefore the phase-sum distribution is a useful tool to probe the nonlinear effects.

The present analysis applies, for the first time, the above phase statistics to the SDSS galaxy catalogs to quantify the non-Gaussianity in galaxy distributions. There are three possible sources of the non-Gaussianity in the present galaxy density field: primordial density field, nonlinear gravitational evolution, and nonlinear galaxy biasing. Recently, WMAP showed that the primordial density field is well approximated by Gaussian statistics. Thus, the primordial non-Gaussianity can be safely ignored in the following analysis, and the prominent source of non-Gaussianity in the galaxy distribution is nonlinear gravitational evolution. In our analysis, we use the phase statistics as a cosmological tool independent of the two-point statistics. We compare the phase correlations of SDSS galaxies with those of mock samples constructed from  $N$ -body simulations based on various cosmological models. For a fair comparison with observations, we consider the observational systematic effects including the survey geometry, the redshift distortion and the shot-noise due to the sparse sampling. We find that the SDSS galaxy data agree very well with the LCDM model predictions with  $\sigma_8 = 0.9$ , which is consistent with the results of WMAP.

Another possible source for non-Gaussianity, galaxy biasing, is the uncertainty of the statistical relation between galaxies and the underlying mass, which originates from complicated processes of galaxy formation. It is known that galaxy clustering depends sensitively on various properties of galaxies, such as the luminosity, color, morphology, and environment (e.g., Dressler 1980). The two-point statistics using SDSS galaxies by Zehavi et al. (2005) and Tegmark et al. (2004a) clearly exhibits the luminosity and morphology dependence of the galaxy biasing (see also Kayo et al. 2004 for the dependence in three-point correlation functions). If the density fluctuation of galaxies,  $\delta_g(\mathbf{x})$ , is related to the mass density fluctuation,  $\delta_m(\mathbf{x})$ , as  $\delta_g = b_1 \delta_m$ , their Fourier transforms also have the linear relationship  $\delta_{g,\mathbf{k}} = b_1 \delta_{m,\mathbf{k}}$ . Decomposing the Fourier wavevectors to the parts of amplitudes and phases, the amplitudes change proportionally to  $b_1$  regardless of the scale; however, the phases are completely preserved under linear biasing. Therefore, the agreement of the observed phase-sum distribution with the simulated predictions suggests that the galaxy biasing is well approximated by the linear relation if a correct cosmological model is assumed. For definiteness, we adopt a quadratic deterministic biasing and put a constraint on the degree of the

**Table 1.** Properties of our volume-limited samples \*.

$M_{r,\min}$	$M_{r,\max}$	$z_{\min}$	$z_{\max}$	$V_{\text{samp}} [(h^{-1}\text{Mpc})^3]$	$N_{\text{gal}}$	$l_{\text{mean}} [h^{-1}\text{Mpc}]$	$L_{\text{box}} [h^{-1}\text{Mpc}]$	Range of $k [2\pi/(h^{-1}\text{Mpc})]$
-22.0	-21.0	0.067	0.153	$2.92 \times 10^7$	34008	9.50	800	0.006–0.11
-21.0	-20.0	0.044	0.103	$9.20 \times 10^6$	44636	5.91	560	0.009–0.16
-20.0	-19.0	0.028	0.067	$2.69 \times 10^6$	23099	4.88	360	0.01–0.25
-19.0	-18.0	0.018	0.044	$7.46 \times 10^5$	8640	4.42	240	0.02–0.37

\* Constructed from the SDSS galaxy catalog ‘Large-scale Structure Sample 15’ in Northern hemisphere. Listed values are the upper and lower limits of the  $r$ -band magnitude,  $M_{r,\min/\max}$ , the upper and lower limits of the redshift,  $z_{\min/\max}$ , the survey volume,  $V_{\text{samp}}$ , the total number of galaxies,  $N_{\text{gal}}$ , the mean separation of galaxies,  $l_{\text{mean}}$ , the box-size for Fourier transform,  $L_{\text{box}}$ , and the scale range of  $k$  in Fourier space to be used in measuring the distribution function of the phase sum. LCDM model parameters,  $\Omega_{\text{m}} = 0.3$  and  $\Omega_{\Lambda} = 0.7$ , are assumed throughout.

nonlinearity of galaxy biasing in a weakly nonlinear regime ( $> 30h^{-1}\text{Mpc}$ ).

This paper is organized as follows. In section 2 we describe the SDSS data sets and our simulation mock catalogs. Section 3 summarizes the perturbative formula of phase-sum distribution by Matsubara (2003) and explains the method of measuring phase correlations using the distribution function of phase sum. The results of observed phase correlations are also presented. Section 4 is focused on the bispectrum analysis of  $p^{(3)}$  from comparison between observations and their mock catalogs. Finally section 5 is devoted to a summary of our results and further discussion.

## 2. Volume-Limited Samples for SDSS Galaxies and Mock Catalogs

Our present analysis is based on a subset of the SDSS galaxy redshift data, ‘Large-scale Structure Sample 15’ (Blanton et al. 2005). This sample includes the spectroscopic data of 389306 galaxies and covers the sky area of 4426 square degrees. The angular selection function of the survey is written in terms of spherical polygons (Hamilton, Tegmark 2004). Details of the SDSS can be found in the following literature: York et al. (2000) provide an overview of the SDSS. Technical articles providing details of the SDSS include descriptions of the photometric camera (Gunn et al. 1998), photometric analysis (Stoughton et al. 2002), the photometric system and photometric calibration (Fukugita et al. 1996; Hogg et al. 2001; Ivezić et al. 2004; Smith et al. 2002), the photometric pipeline (Lupton et al. 2001), astrometric calibration (Pier et al. 2003), selection of the galaxy spectroscopic samples (Eisenstein et al. 2001; Strauss et al. 2002), and spectroscopic tiling (Blanton et al. 2003a). The details of publicly released data are summarized in Stoughton et al. (2002) for Early Data Release and Abazajian et al. (2003, 2004, 2005) for Data Release One, Two and Three, respectively.

In our analysis we use observational data in the Northern hemisphere, except for the distant area from the other observed areas, which is designed to overlap with the Spitzer Space Telescope First Look Survey. We also omit the area of three stripes in the Southern hemisphere, which has a survey geometry not appropriate

for the analysis of galaxy clustering in three-dimensional space. The range of the  $r$ -band apparent magnitude ( $m_{r,\min}, m_{r,\max}$ ) is set to be a conservative range of (14.5, 17.5) after correction for Galactic reddening using the maps of Schlegel, Finkbeiner, and Davis (1998). We construct four volume-limited samples with a unit width of the absolute magnitude, which cover the range of the  $r$ -band absolute magnitude from  $-22$  to  $-18$  (Table 1). The redshift range of each volume-limited sample ( $z_{\min}, z_{\max}$ ) is determined by the following distance modulus relation:

$$M_{r,\min/\max} = m_{r,\min/\max} - 5 \log[r_{\min/\max}(1 + z_{\min/\max})/10 \text{ pc}] - K(z_{\min/\max}), \quad (2)$$

where  $r_{\min/\max}$  is the comoving distance at a redshift of  $z_{\min/\max}$  and  $K(z)$  is a quadratic fitting formula of the averaged  $K$ -correction as a function of  $z$  (Park et al. 2005),

$$K(z) = 2.3537z^2 + 0.5735z - 0.18437. \quad (3)$$

The details of  $K$ -correction is described in Blanton et al. (2003b). Table 1 summarizes the properties of our volume-limited subsamples.

For a fair comparison with the observation, we construct a set of mock simulation data, including observational effects of the survey geometry, the number density, and the redshift distortion (Hikage et al. 2002, 2003). For constructing mock samples, we use P<sup>3</sup>M  $N$ -body simulations, provided by Jing and Suto (1998). The simulation employs  $256^3$  particles in a periodic comoving box with a length of  $300h^{-1}\text{Mpc}$  or  $600h^{-1}\text{Mpc}$  using Gaussian initial conditions and a Cold Dark Matter (CDM) transfer function (Bardeen et al. 1986). We use the  $z = 0$  snapshot simulation data (for simplicity we neglect the light-cone effect) in various CDM models with the parameters listed in Table 2; the dimensionless matter-density parameter,  $\Omega_{\text{m}}$ , the dimensionless cosmological constant,  $\Omega_{\Lambda}$ , the shape parameter,  $\Gamma$  of the CDM transfer function (Bardeen et al. 1986), and the r.m.s. density-fluctuation amplitude smoothed by a top-hat filter with a scale of  $8h^{-1}\text{Mpc}$ ,  $\sigma_8$ . We extract about 10 realizations of wedge samples for each volume-limited sample out of the full simulation cube so that they have the same sample-shape and number of particles (averaged over mock samples) as each volume-limited sample. To construct mock samples

that extend beyond the simulation box size, we duplicate particles using the periodic boundary conditions. We create mock data in redshift space by adding the line-of-sight component of the peculiar-velocity to the distance of each particle for calculating redshift. The mock sample simply assumes that each mass particle represents a simulated galaxy, and neglects the effect of galaxy biasing, which are further discussed in section 4.

**Table 2.** Simulation model parameters

Model	$\Omega_m$	$\Omega_\Lambda$	$\Gamma$	$\sigma_8$
$\Lambda$ CDM	0.3	0.7	0.21	1, 0.9, 0.7
SCDM	1	0	0.5	0.6
OCDM	0.3	0	0.25	1

### 3. The Distribution Function of Phase Sum

Matsubara (2003) derived an analytical relation between the polyspectra and the distribution of the phase sum in perturbation theory. In the lowest-order approximation, the probability density function (PDF) of the phase sum,  $\theta_{\mathbf{k}_1} + \theta_{\mathbf{k}_2} - \theta_{\mathbf{k}_1+\mathbf{k}_2}$ , over closed wavevectors  $\mathbf{k}_1, \mathbf{k}_2$ , and  $-\mathbf{k}_1 - \mathbf{k}_2$  reduces to (Matsubara 2003):

$$\mathcal{P}(\theta_{\mathbf{k}_1} + \theta_{\mathbf{k}_2} - \theta_{\mathbf{k}_1+\mathbf{k}_2} | V_{\text{samp}}) \propto 1 + \frac{\pi^{3/2}}{4} p^{(3)}(\mathbf{k}_1, \mathbf{k}_2 | V_{\text{samp}}) \cos(\theta_{\mathbf{k}_1} + \theta_{\mathbf{k}_2} - \theta_{\mathbf{k}_1+\mathbf{k}_2}), \quad (4)$$

where  $V_{\text{samp}}$  is the sampling volume and  $p^{(3)}$  is defined by the bispectrum,  $B(\mathbf{k}_1, \mathbf{k}_2)$ , and the power spectrum,  $P(k)$ , as follows:

$$p^{(3)}(\mathbf{k}_1, \mathbf{k}_2 | V_{\text{samp}}) = \frac{B(\mathbf{k}_1, \mathbf{k}_2)}{\sqrt{V_{\text{samp}} P(k_1) P(k_2) P(|\mathbf{k}_1 + \mathbf{k}_2|)}}. \quad (5)$$

In the lowest-order approximation, the PDF of the phase sum over three wavevectors is fully determined by the parameter  $p^{(3)}$ . If the hierarchical clustering ansatz is valid,  $B \sim P^2$  and thereby  $p^{(3)}$  is approximately given by  $\sqrt{P/V_{\text{samp}}}$ . Therefore, the lowest-order approximation [equation (4)] breaks down at a scale  $k$  satisfying the condition  $P(k)/V_{\text{samp}} > 1$ . Note that this is different from the conventional condition of the gravitational nonlinear clustering,  $k^3 P(k) > 1$ . In fact, a subsequent numerical analysis confirmed the validity of the perturbative formula, even in a fairly nonlinear regime of clustering (Hikage et al. 2004).

The dependence of the phase-sum distribution on the sampling volume can be naturally explained as follows: the synchronization of phases becomes weak when multiple density peaks with comparable heights exist (section 1). Because the sampling volume is larger, the number of peaks increases, and thus the phase-sum distribution approaches being uniform.

When  $V_{\text{samp}}$  is sufficiently large, the higher order terms above  $p^{(3)}$  become negligible and then equation (4) is applicable, even in nonlinear regimes, in the sense that

$k^3 P(k) > 1$ . On the contrary, decreasing  $V_{\text{samp}}$  by dividing the original survey volume into several sub-volumes would provide information about the higher-order spectrum. Dividing the original sample, however, leads to decreasing the number of objects per sub-sample. Thus, a significant fraction of the available Fourier modes suffers from the contamination of shot noise. In the present galaxy sample, it is quite difficult to extract higher order information beyond  $p^{(3)}$  from the distribution function of the three-point phase sum. In the present work, therefore, we do not divide the survey volume of each volume-limited sample.

We compute the distribution function of the phase sum for density contrast fields from mock samples and SDSS galaxies. We use the cloud-in-cell interpolation to assign galaxies or dark matter particles to mesh densities. Then, the density contrast field is Fourier-transformed on cubic grids with a mesh number  $N_{\text{mesh}} = 256$  per side. We calculate the sum of the Fourier phases for the closed set of three wavevectors, and then compute the distribution function of the phase sum within each binning range of triangle configurations. For simplicity, we focus on the configuration of wavevectors to be a nearly isosceles triangle, where the absolute values of two wavevectors,  $k_1$  and  $k_2$ , are within the same binning range of scale  $k$ . The scale  $k$  is divided into 8 bins with equal width in logarithmic scale in the range of  $a < k/k_{\text{Nyq}} < b$ . The Nyquist frequency  $k_{\text{Nyq}}$  is equal to  $2\pi \times (N_{\text{mesh}}/2)/L_{\text{box}}$ , where  $L_{\text{box}}$  is a side of a cubic box for a Fourier transformation. Table 1 lists  $L_{\text{box}}$  for each volume-limited sample, which is chosen for the sample volume to be barely covered. We limit the range of scale to be  $a = 0.04$  and  $b = 0.7$  so that the observational systematics due to the complicated survey geometry and the discreteness effect may be neglected compared to the sample variance; at smaller  $k$ , the Poisson error increases due to the limited number of independent combinations of modes forming closed triangles, and furthermore the convolution effect with the survey mask is more serious. At larger  $k$ , the shot noise becomes more serious. Table 1 lists the range of scale  $k$  for each volume-limited sample. The unit of scale  $k$  in Fourier space is set to be  $2\pi/(h^{-1}\text{Mpc})$ , and thereby the corresponding scale-length in real space is just the inverse of  $k$  in units of  $h^{-1}\text{Mpc}$ . The angle  $\varphi$  between  $\mathbf{k}_1$  and  $\mathbf{k}_2$ , i.e.,  $\varphi \equiv \arccos[(\mathbf{k}_1/k_1) \cdot (\mathbf{k}_2/k_2)]$  with  $0^\circ < \varphi < 180^\circ$ , is binned to have an equal width of  $20^\circ$ .

Figure 1 plots the distribution function of the phase sum for each volume-limited sample in symbols. For comparison, we plot in lines the lowest-order approximation [equation (4)] using  $p^{(3)}$  computed from the bispectrum and the power spectrum (5). In the left panels, the triangle configurations are nearly equilateral shape ( $110^\circ < \varphi < 130^\circ$ ) for different  $k$ . In the right panels, the triangle configurations are nearly isosceles for different angles,  $\varphi$ . The phase-sum distributions are found to be well approximated by the lowest-order approximation for all of the volume-limited samples, regardless of the triangle configurations. The dependence of  $p^{(3)}$  on  $V_{\text{samp}}$  and  $k$  can be understood from the nature of perturbative parameter,  $p^{(3)}$ , which is roughly proportional to  $[P(k)/V_{\text{samp}}]^{1/2}$  under the hi-



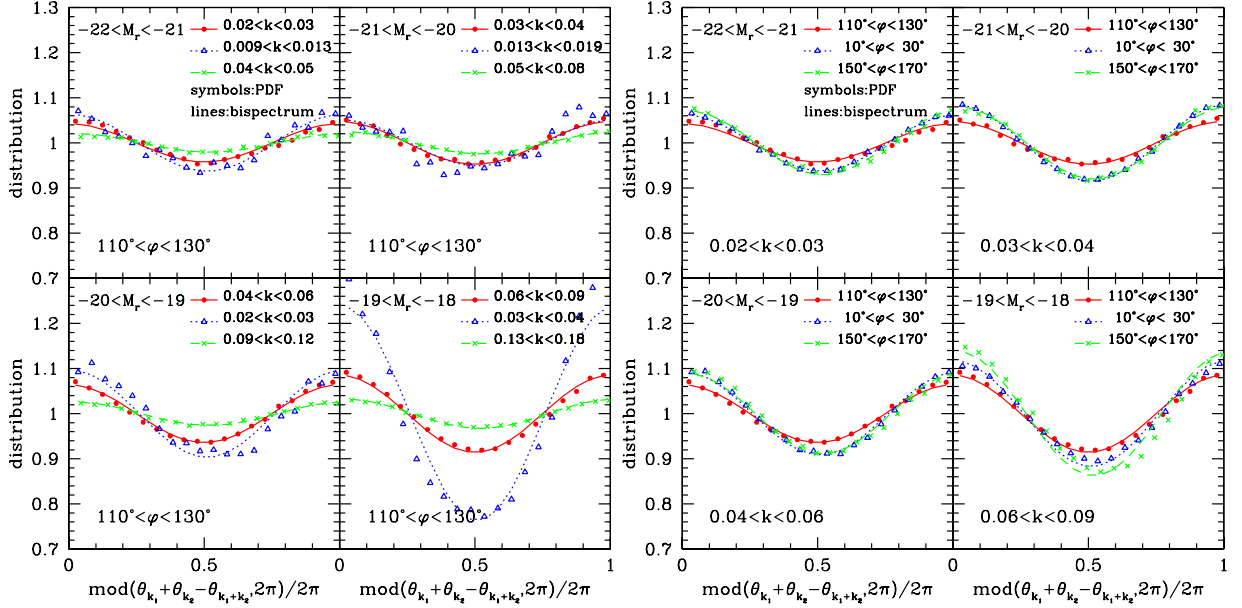


**Fig. 1.** Comparison of the observed distribution function of the phase sum (symbols) with the lowest-order approximation [equation (4)] where  $p^{(3)}$  is computed by the combination of the bispectrum and the power spectrum from observations [equation (5)] (lines). Different panels show the results for different volume-limited samples. In left figure, the configurations of triangle wavevectors are focused on nearly equilateral triangle ( $110^\circ < \varphi < 130^\circ$ ) with different scales of  $k \sim k_1 \sim k_2$ . In right figure, the triangle configurations are nearly isosceles ( $k \sim k_1 \sim k_2$ ) with different angles  $\varphi$  between  $k_1$  and  $k_2$ . The unit of scale  $k$  is set to be  $2\pi/(h^{-1}\text{Mpc})$ .

erarchical clustering ansatz; volume-limited samples for fainter galaxies have a smaller  $V_{\text{samp}}$  (increase  $p^{(3)}$ ), but a smaller  $P(k)$  (decrease  $p^{(3)}$ ) because the measurable range of scale  $k$  is shifted to larger values due to the smaller  $V_{\text{box}}$ . The redshift distortion due to the random motion of galaxies also smears the power at small scales, and thus  $p^{(3)}$  reaches up to 0.3 at a maximum, much smaller than unity. Figure 1 shows that  $p^{(3)}$  calculated from the amplitude of the phase-sum distribution using equation (4) is nearly equal to that from the combination of the bispectrum and the power spectrum [equation (5)]. In what follows, we will use equation (5) to compute  $p^{(3)}$  instead of fitting the PDF to equation (4).

#### 4. Bispectrum Analysis of $p^{(3)}$

Figures 2 and 3 show  $p^{(3)}$  for SDSS galaxies in different volume-limited samples (plotted in symbols) against the wavenumber  $k$  (Figure 2) and the angle  $\varphi$  (Figure 3). For comparison, the LCDM predictions with  $\sigma_8 = 0.9$  are plotted in lines. Clearly, the scale-dependence of  $p^{(3)}$  is well approximated by a power-law of  $k$ . This can be understood again from equation (5); because  $B(k_1, k_2)$  and  $P(k)$  may be approximated as power-laws at those scales, we expect  $p^{(3)} \propto \sqrt{P(k)} \propto k^{-1}$ . The right panels show the ratio of the observed  $p^{(3)}$  to the corresponding mock estimations in the left panels. The overall agreement between observations and LCDM predictions with  $\sigma_8 = 0.9$  is very good.

Figures 4 and 5 show comparisons of the observed  $p^{(3)}$  with various mock predictions to examine the cosmology dependence. Figure 4 focuses on the scale dependence,

while Figure 5 focuses on the shape dependence (the angle  $\varphi$  of the triangles). The right panels show the ratio of  $p^{(3)}$  between observations and the corresponding mock samples in the left panels. Again, LCDM predictions with  $\sigma_8 = 0.9$  show the best agreement with the observations among our mock samples; the SCDM model predicts a smaller  $p^{(3)}$  than the other models over the whole range of scales, mainly because of the smaller value of  $\sigma_8$  (see Table 2). The OCDM model has the same value of  $\sigma_8$  as the LCDM models, but their spectral shape is different: the small-scale fluctuation in OCDM is slightly larger due to the larger value of  $\Gamma$ , and thus OCDM predicts higher values of phase correlations than LCDM. Figures 6 and 7 are same as Figures 4 and 5, but for the  $\sigma_8$  dependence using mock samples based on the same cosmology of LCDM. A systematic increase of  $p^{(3)}$  as  $\sigma_8$  is clearly found because the phase correlations become strong as the gravitational evolution proceeds.

Galaxy biasing is another source of uncertainty in comparing the observations and the mock predictions. If the galaxy biasing is linear, i.e.,  $\delta_g = b_1 \delta_m$ , the amplitude changes in proportion to the linear coefficient,  $b_1$ , but the phases are invariant. Thus, the consistency of the LCDM model remains valid as long as the galaxy biasing is well approximated by the linear relation in *redshift* space (note that this does not strictly correspond to the linear biasing in *real* space). The analysis of the bispectrum for 2dFGRS finds that galaxy biasing is consistent to be linear under LCDM model in the range of scales from  $5h^{-1}\text{Mpc}$  to  $30h^{-1}\text{Mpc}$  (Verde et al. 2002).

Indeed, the combined analysis of three-point correlation functions and two-point correlation functions shows a sig-

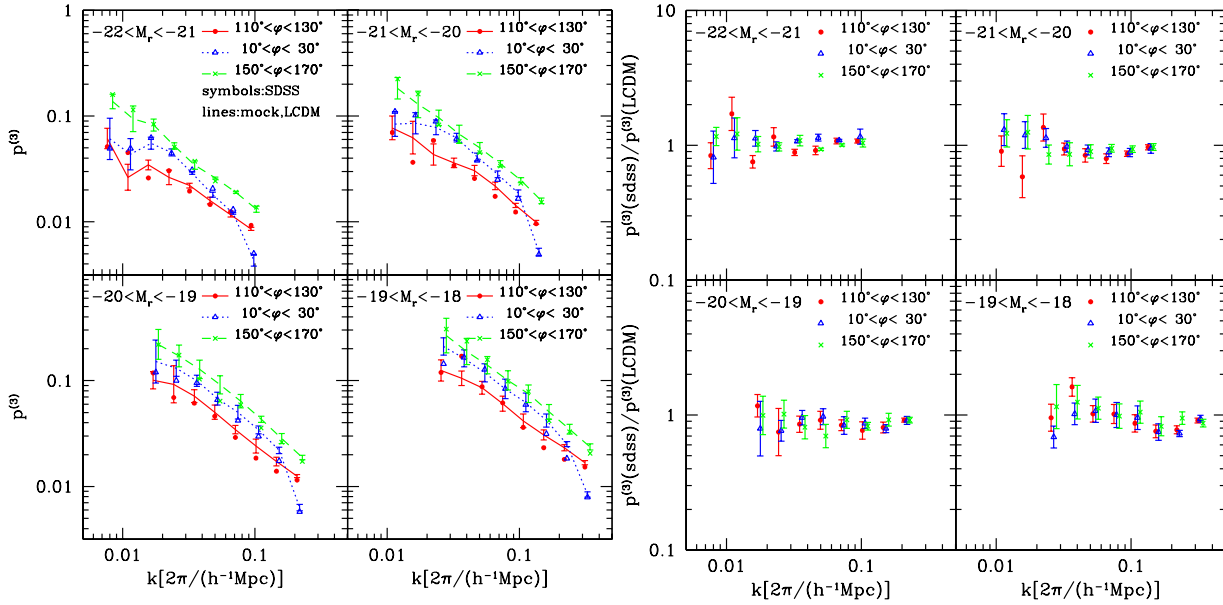


**Fig. 2.** Scale dependence of the observed  $p^{(3)}$  for each volume-limited sample (symbols). For comparison, the estimations of mock samples based on the representative model of LCDM with  $\sigma_8 = 0.9$  are plotted by lines. The right figures show the ratio of the observed  $p^{(3)}$  and the corresponding mock estimations. The configurations of triangle wavevectors are equilateral triangles with different scales of  $k$ . Error-bars represent the sample variance of the mock samples for each sample.

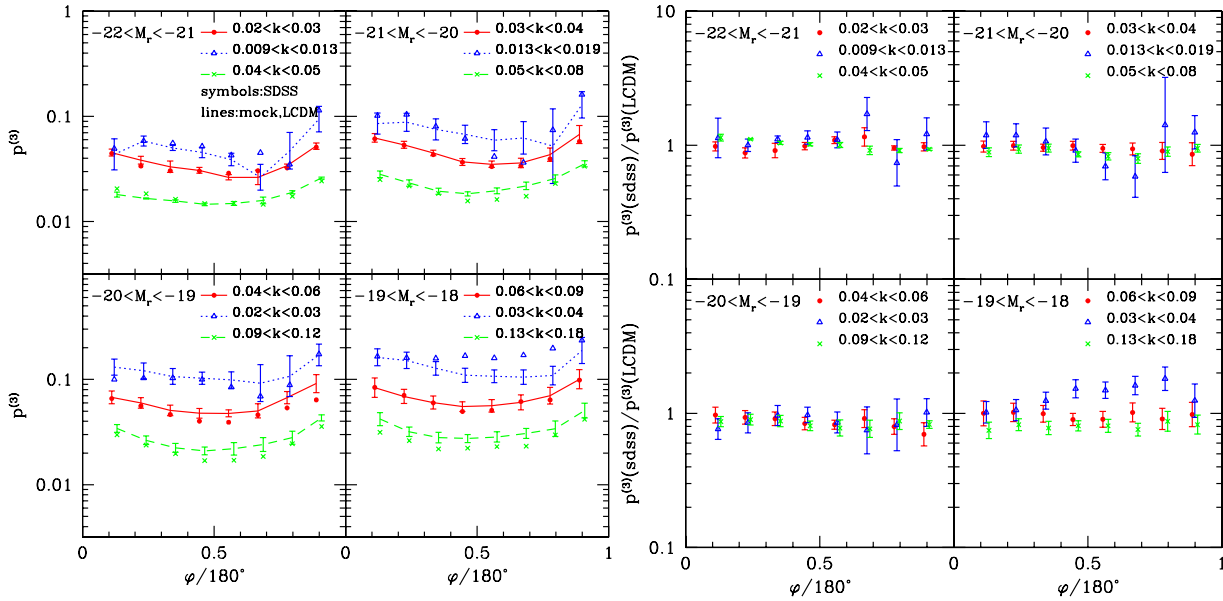


**Fig. 3.** Same as Figure 2, but for the angle  $\varphi$  dependence. The configurations of triangle wavevectors are isosceles with different  $\varphi$ .

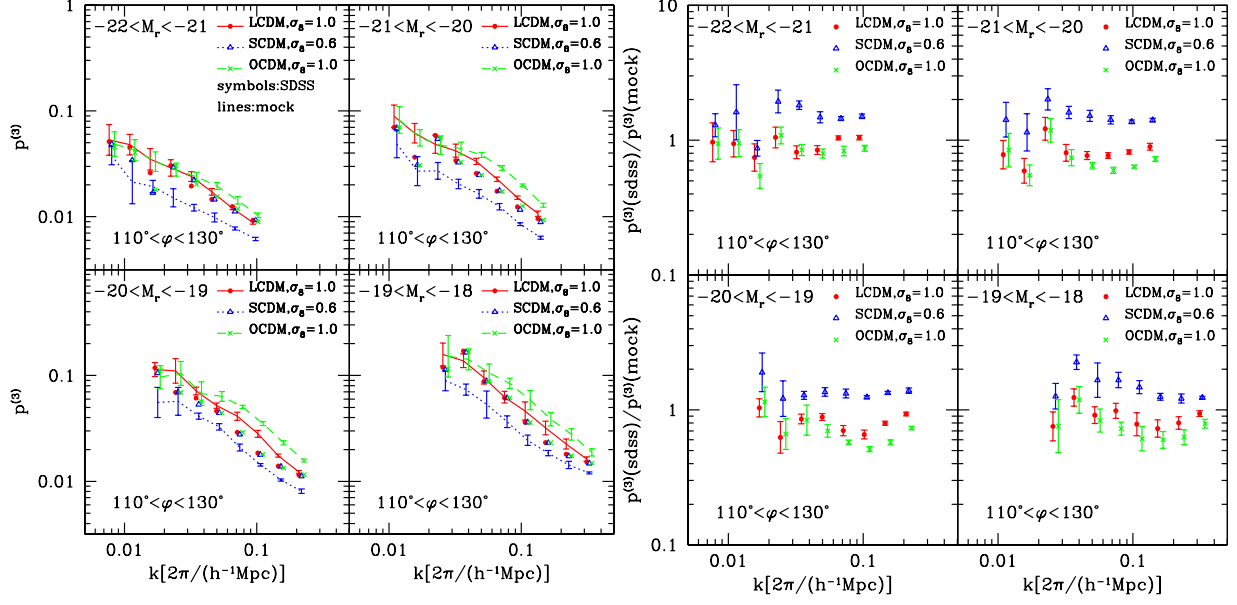


**Fig. 4.** Comparison of the observed  $p^{(3)}$  (symbols) with the simulated estimations (lines) based on various cosmologies, in particular focused on the scale dependence; LCDM with  $\sigma_8 = 1$  (filled circles and solid lines), SCDM (open triangles and dotted lines), and OCDM ( $\sigma_8 = 1.0$  (crosses and dashed lines)). The right figures show the ratio of the observed  $p^{(3)}$  to the simulated  $p^{(3)}$  for each cosmology corresponding to the left figures. The error-bars represent the sample variance of the mock samples. The configuration formed by three wavevectors is in the shape of nearly equilateral triangles ( $110^\circ < \varphi < 130^\circ$ ).

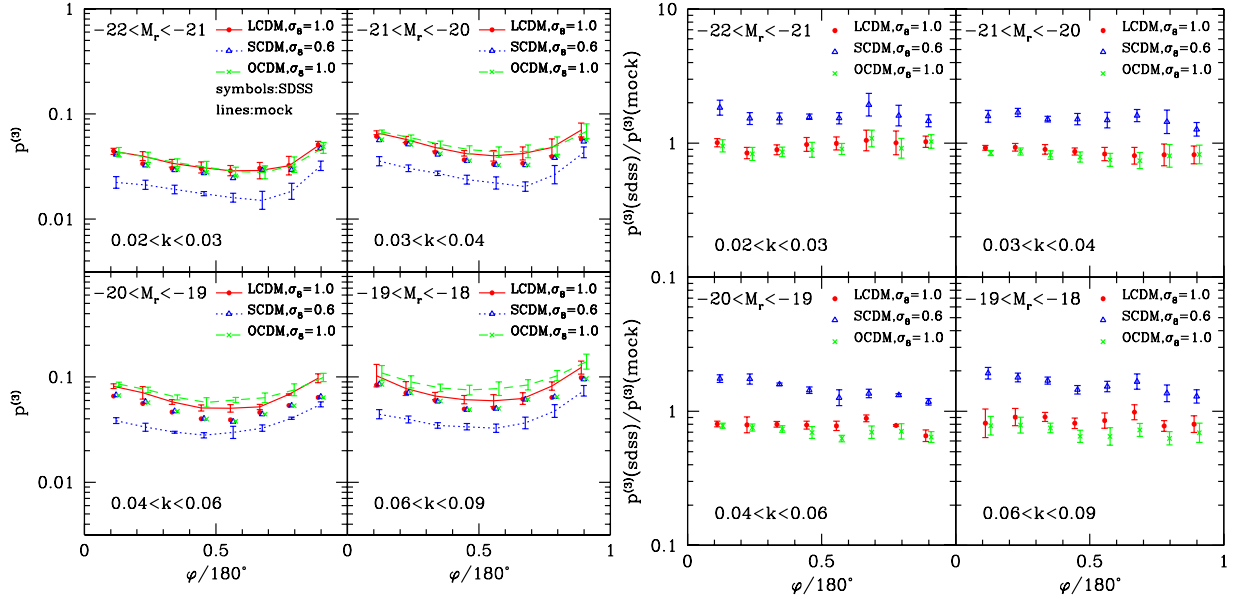


**Fig. 5.** Same as Figure 4, but for angle  $\varphi$  dependence. The configuration of the triangle is isosceles ( $k_1 \sim k_2 \sim k$ ) and thus the plotted scale is within the intermediate bin of scales for each volume-limited sample.

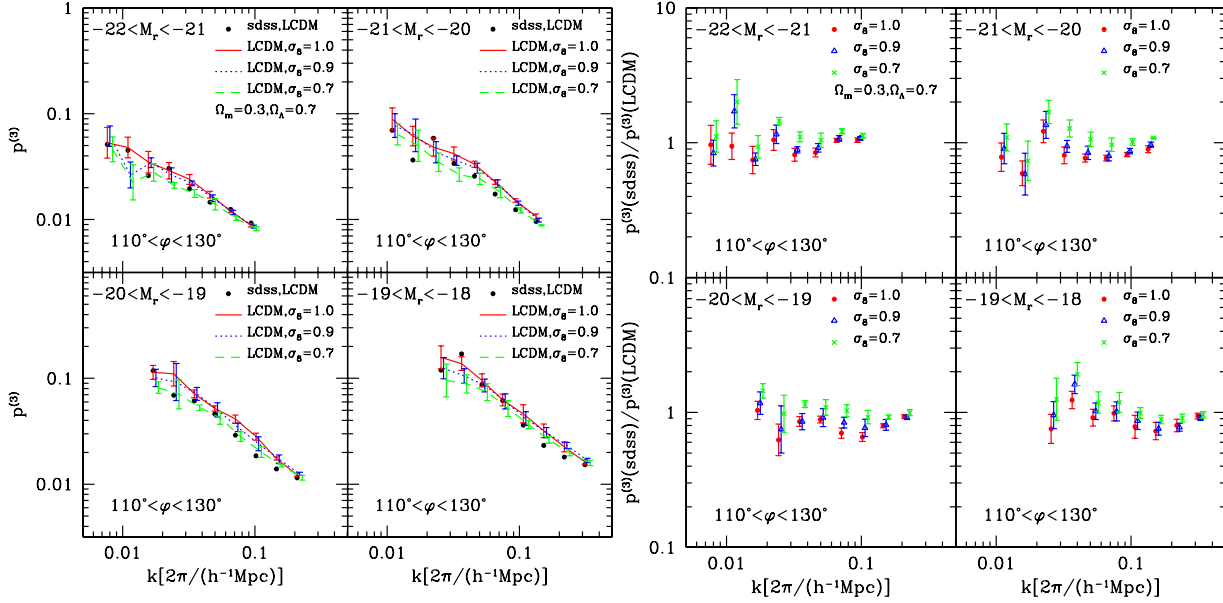


**Fig. 6.** Same as Figure 4, but for compared mock samples based on LCDM models with  $\sigma_8 = 1$  (filled circles and solid lines),  $\sigma_8 = 0.9$  (open triangles and dotted lines), and  $\sigma_8 = 0.7$  (crosses and dashed lines).

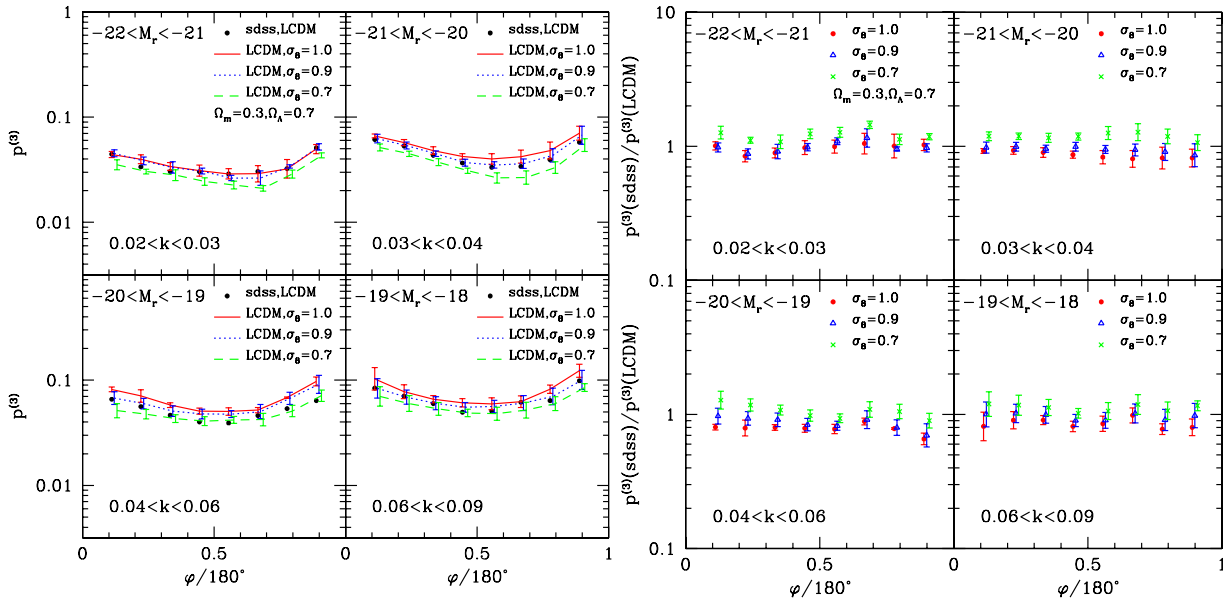


**Fig. 7.** Same as Figure 6, but for the angle  $\varphi$  dependence. The configuration of the triangle is isosceles ( $k_1 \sim k_2 \sim k$ ), and thus the plotted scale is within the intermediate bin of scales for each volume-limited sample.



nificant deviation from linear biasing at *nonlinear* scales from  $1h^{-1}\text{Mpc}$  to  $10h^{-1}\text{Mpc}$  (Kayo et al. 2004). In contrast, the scales that we probe in the present analysis is much larger, i.e.,  $> 30h^{-1}\text{Mpc}$ . We therefore parameterize the galaxy biasing by the local and quadratic relation between the density fluctuation of galaxies,  $\delta_g$ , and that of mass,  $\delta_m$ , as follows;

$$\delta_g = b_1 \delta_m + \frac{b_2}{2} (\delta_m^2 - \langle \delta_m^2 \rangle), \quad (6)$$

where  $b_1$  and  $b_2$  are biasing parameters. In a weakly nonlinear regime, for example at scales larger than  $30h^{-1}\text{Mpc}$ , the locality of the galaxy biasing is valid because the scale of galaxy formation is much smaller ( $\sim \text{Mpc}$ ). Also the density fluctuation is less than unity, and thereby higher order terms of the density fluctuation are negligible. Under the above quadratic biasing,  $p_g^{(3)}$  for galaxies and  $p_m^{(3)}$  for mass are related as

$$p_g^{(3)}(\mathbf{k}_1, \mathbf{k}_2) = p_m^{(3)}(\mathbf{k}_1, \mathbf{k}_2) + \frac{b_2}{b_1} f(P_1, P_2, P_3), \quad (7)$$

$$f(P_1, P_2, P_3) = \frac{P_1 P_2 + P_2 P_3 + P_3 P_1}{\sqrt{V_{\text{samp}} P_1 P_2 P_3}}, \quad (8)$$

where  $P_1 = P(k_1)$ ,  $P_2 = P(k_2)$ , and  $P_3 = P(|\mathbf{k}_1 + \mathbf{k}_2|)$ . Equation (7) implies that the difference of  $p_g^{(3)}$  from  $p_m^{(3)}$  is proportional to the ratio  $b_2/b_1$  alone.

Figure 8 plots  $b_2/b_1$  calculated from the difference between  $p_g^{(3)}$  and  $p_m^{(3)}$  for each cosmology using equation (7). The plotted values of  $b_2/b_1$  are averaged over scales larger than  $30h^{-1}\text{Mpc}$  ( $k < 0.03[2\pi/(h^{-1}\text{Mpc})]$ ). In constraining  $b_2/b_1$ , we do not use the phase sum for the configuration of triangle wavevectors with the opening angle,  $\varphi < 90^\circ$ , because we find that they strongly suffer from the observational systematic due to the survey geometry beyond the sample variance. We note that the ratio of the biasing parameters in Figure 8 is calculated from the density field in redshift space and thus their values are quantitatively different in real space.

The results in Figure 8 suggest that the nonlinearity of the galaxy biasing,  $b_2/b_1$ , is generally rather small and simply dependent on  $\sigma_8$ , regardless of the cosmology and galaxy luminosity. We thereby plot the relation between  $\sigma_8$  and  $b_2/b_1$  averaged over all of four volume-limited samples in Figure 9. Indeed, we find that  $\sigma_8$  mainly determines the resulting  $b_2/b_1$  regardless of cosmology at scales  $> 30h^{-1}\text{Mpc}$ , and that their relation is well fitted by the following linear relation:

$$b_2/b_1 = (0.54 \pm 0.06) - (0.62 \pm 0.08)\sigma_8. \quad (9)$$

The linear relation is valid if  $|b_2/b_1| \ll 1$  and the power spectrum of the mass fluctuation is mainly determined by the square of  $\sigma_8$  at  $> 30h^{-1}\text{Mpc}$ ; both  $p_m^{(3)}$  and  $f$  (equation 7) are roughly given by  $\sqrt{P/V_{\text{samp}}}$ , which is proportional to  $\sigma_8$  in a nearly linear regime. Thus,  $b_2/b_1$  is linearly related to  $\sigma_8$  as long as  $|b_2/b_1|$  is much smaller than unity.

When we adopt a value of  $\sigma_8 \sim 0.9$ , measured from the combined analysis of recent WMAP results and the power

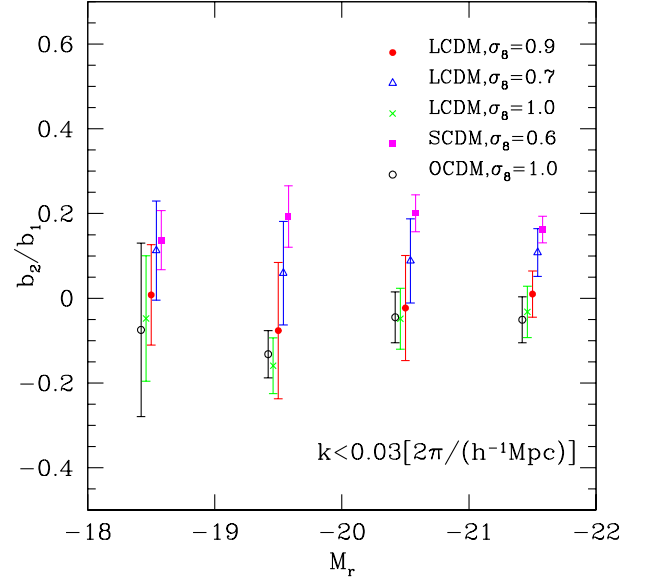


**Fig. 8.** Averaged ratio of the quadratic bias parameter to the linear bias parameter,  $b_2/b_1$ , estimated from the difference of  $p^{(3)}$  between observations and mock predictions using equation (7). Cosmological models used in mock predictions are LCDM with  $\sigma_8 = 0.9$  (filled circles), LCDM with  $\sigma_8 = 0.7$  (open triangles), LCDM with  $\sigma_8 = 1.0$  (crosses), SCDM (filled squares), and OCDM (open circles). Averaging is performed over various configurations of triangles with all of scales of three wavevectors ( $k_1$ ,  $k_2$ , and  $|k_1 + k_2|$ ) less than  $0.03[2\pi/(h^{-1} \text{Mpc})]$  and  $\varphi > 90^\circ$ . The error-bars represent the sample variance of the mock predictions.

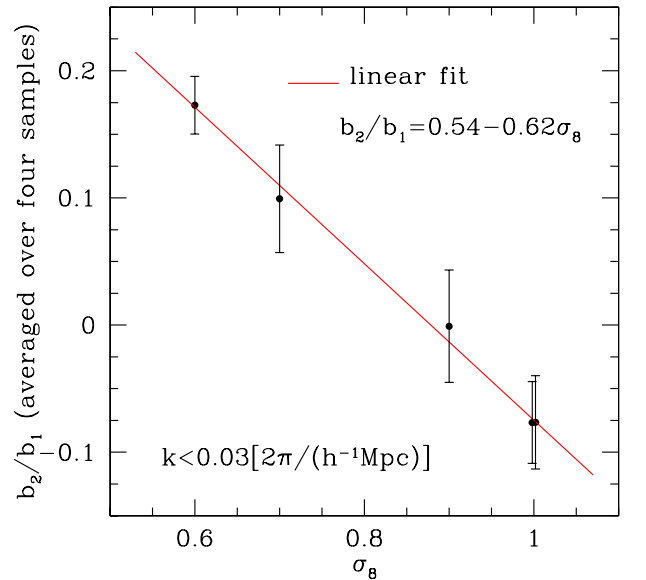


**Fig. 9.** Relation between  $\sigma_8$  of assumed cosmologies for mock samples and the averaged  $b_2/b_1$  over all four volume-limited samples under the corresponding cosmologies, which are plotted in Figure 8. The plotted line represents the best fit of the above relation with a linear function,  $b_2/b_1 = A + B\sigma_8$ , where  $A = 0.54(\pm 0.06)$  and  $B = -0.62(\pm 0.08)$ . The error-bars represent the sample variance of the mock predictions.

spectrum of SDSS galaxies (Spergel et al. 2003; Tegmark et al. 2004b),  $b_2/b_1 = -0.02 \pm 0.1$ . Therefore, we conclude that the galaxy biasing is well approximated by a linear relation. Complementary measurements of  $\sigma_8$  from other observations which are independent of the galaxy biasing, including weak gravitational lensing and galaxy clusters, will put additional constraints on the nonlinearity of the galaxy biasing.

## 5. Summary and Conclusions

We have performed the first measurement of the distribution function of the phase sum of galaxies. We applied the phase statistics to volume-limited samples of the latest SDSS galaxy catalogs. We found that the distribution functions of the phase sum for all of the SDSS galaxy samples are in good agreement with the lowest-order perturbation formula. Since the latter is characterized by  $p^{(3)}$ , we explored various properties of  $p^{(3)}$ . For a quantitative comparison with observations, we constructed realistic mock catalogs from  $N$ -body simulations. We found that the observational phase correlations agree best with the LCDM model with  $\sigma_8 = 0.9$  if galaxy biasing is linear; the SCDM model predicts weaker correlations of phases than observations overall, mainly due to the small  $\sigma_8$ . Actually, we found a systematic increase of  $p^{(3)}$  as  $\sigma_8$  increases with the same parameters of the LCDM model.

Assuming that galaxy biasing is expressed by a quadratic deterministic relation in a weakly nonlinear regime ( $k < 0.03[2\pi/(h^{-1}\text{Mpc})]$ ), we placed constraints on a linear combination of the nonlinearity in the galaxy biasing  $b_2/b_1$  and  $\sigma_8$  as  $b_2/b_1 = 0.54(\pm 0.06) - 0.62(\pm 0.08)\sigma_8$ . Using a recent measurements of  $\sigma_8 \sim 0.9$  from a combined analysis of WMAP and SDSS, the galaxy biasing was found to be well approximated by a linear relation.

In the present analysis, we have focused on the behavior of  $p^{(3)}$ , which carries phase information contained in the bispectrum (Scoccimarro et al. 2001; Scoccimarro 2000). In this sense, our analysis is equivalent to an analysis of the bispectrum, which is also a first attempt using SDSS data. Higher order information beyond bispectrum can be obtained by measuring the distribution function of the phase sum over more than four numbers of wavevectors which form closed polygons. Another approach is to decrease  $V_{\text{samp}}$ , because the perturbative parameter,  $p^{(3)}$ , is inversely proportional to  $\sqrt{V_{\text{samp}}}$ . However, extracting higher order information is limited mainly by the shot noise, as discussed in section 3. Therefore, deeper and denser surveys than SDSS are required to carry out this attempt in reality.

We deeply appreciate I. Kayo and Y. P. Jing who kindly provided a large set of  $N$ -body simulation data. C. H. acknowledges support from a JSPS (Japan Society for the Promotion of Science) fellowship. T. M. acknowledges the support from the Ministry of Education, Culture, Sports, Science, and Technology, Grant-in-Aid for Encouragement of Young Scientists (No. 15740151). The research of Y.S. was supported in part by Grants-

in-Aid for Scientific Research from the Japan Society for Promotion of Science (Nos.14102004 and 16340053). Numerical computations were carried out at ADAC (the Astronomical Data Analysis Center) of the National Astronomical Observatory, Japan (project ID: yys08), and also at computer facilities at the University of Tokyo supported by the Special Coordination Fund for Promoting Science and Technology, Ministry of Education, Culture, Sport, Science and Technology.

Funding for the Sloan Digital Sky Survey (SDSS) has been provided by the Alfred P. Sloan Foundation, the Participating Institutions, the National Aeronautics and Space Administration, the National Science Foundation, the U.S. Department of Energy, the Japanese Monbukagakusho, the Max Planck Society, and the HEFCE. The SDSS Web site is <http://www.sdss.org/>.

The SDSS is a joint project of The University of Chicago, Fermilab, the Institute for Advanced Study, the Japan Participation Group, The Johns Hopkins University, the Korean Scientist Group, Los Alamos National Laboratory, the Max-Planck-Institute for Astronomy (MPIA), the Max-Planck-Institute for Astrophysics (MPA), New Mexico State University, University of Pittsburgh, University of Portsmouth, Princeton University, the United States Naval Observatory, and the University of Washington.

## References

- Abazajian, K., et al. 2003, AJ, 126, 2081 (Data Release One)
- Abazajian, K., et al. 2004, AJ, 128, 502 (Data Release Two)
- Abazajian, K., et al. 2005, AJ, 129, 1755 (Data Release Three)
- Bardeen, J. M., Bond, J. R., Kaiser, N., & Szalay, A. S. 1986, ApJ, 304, 15
- Barrow, J. D., Bahavsar, S. P., & Sonoda, D. H. 1985, MNRAS, 216, 17
- Bertschinger, E., 1992 in Lecture Notes in Physics, 408, New Insights into the Universe, ed. V. Martinez, M. Portilla, & D. Saez (Berlin:Springer-Verlag), 65
- Blanton, M. R., Lin, H., Lupton, R. H., Maley, F. M., Young, N., Zehavi, I., & Loveday, J. 2003, AJ, 125, 2276
- Blanton, M. R., et al. 2003, AJ, 125, 234
- Blanton, M. R., et al. 2005, AJ, 129, 2562
- Chiang, L-Y. 2001, MNRAS, 325, 405
- Chiang, L-Y., Coles, P., & Naselsky, P. 2002, MNRAS, 337, 488
- Coles, P., & Chiang, L-Y. 2000, Nature, 406, 376
- Dressler, A. 1980, ApJ, 236, 351
- Eisenstein, D. J., et al. 2001, AJ, 122, 2267
- Fukugita, M., Ichikawa, T., Gunn, J. E., Doi, M., Shimasaku, K., & Schneider, D. P. 1996, AJ, 111, 1748
- Gott, J. R., III, Melott, A. L., & Dickinson, M. 1986, ApJ, 306, 341
- Gunn, J. E., et al. 1998, AJ, 116, 3040
- Hamilton, A. J. S., & Tegmark, M. 2004, MNRAS, 349, 115
- Hikage, C., 2002, PASJ, 54, 707
- Hikage, C., 2003, PASJ, 55, 911
- Hikage, C., Matsubara, T., & Suto, Y. 2004, ApJ, 600, 553
- Hogg, D. W., Finkbeiner, D. P., Schlegel, D. J., & Gunn, J. E. 2001, AJ, 122, 2129
- Hoyle, F., et al. 2002, ApJ, 580, 663

- Ivezić, Ž., et al. 2004, *Astron. Nachr.*, 325, 583
- Jain, B., & Bertschinger, E. 1998, *ApJ*, 509, 517
- Jing, Y. P., & Suto, Y. 1998, *ApJ*, 494, L5
- Kayo, I., et al. 2004, *PASJ*, 56, 415
- Komatsu, E., et al. 2003, *ApJS*, 148, 119
- Lupton, R., Gunn, J. E., Ivezić, Ž., Knapp, G. R., Kent, S., & Yasuda, N. 2001, in *ASP Conf. Ser. 238, Astronomical Data Analysis Software and Systems X*, ed. F. R. Harnden, Jr., F. A. Primini, and H. E. Payne (San Francisco: Astr. Soc. Pac.) 269
- Matsubara, T. 2003, *ApJ*, 591, L79
- Mecke, K. R., Buchert, T., & Wagner, H. 1994, *A&A*, 288, 697
- Park, C., et al. 2005, *ApJ*, in press (astro-ph/0507059)
- Peebles, P. J. E. 1980, *The Large-Scale Structure of the Universe* (Princeton: Princeton University Press)
- Pier, J., Munn, J. A., Hindsley, R. B., Hennessy, G. S., Kent, S. M., Lupton, R. H., Ivezić, Ž., for the SDSS collaboration, 2003, *AJ*, 125, 1559
- Ryden, B. S., & Gramann, M. 1991, *ApJ*, 383, L33
- Scherrer, R. J., Melott, A. L., & Shandarin, S. F. 1991, *ApJ*, 377, 29
- Schlegel, D. J., Finkbeiner, D. P., & Davis, M. 1998, *ApJ*, 500, 525
- Scoccimarro, R. 2000, *ApJ*, 544, 597
- Scoccimarro, R., Feldman, H. A., Fry, J. N., & Frieman, J. A. 2001, *ApJ*, 546, 652
- Smith, J. A., et al. 2002, *AJ*, 123, 2121
- Soda, J., & Suto, Y. 1992, *ApJ*, 396, 379
- Spergel, D. N., et al. 2003, *ApJS*, 148, 175
- Stoughton, C., et al. 2002, *AJ*, 123, 485 (Early Data Release)
- Strauss, M. A., et al. 2002, *AJ*, 124, 1810
- Suginohara, T., & Suto, Y. 1991, *ApJ*, 371, 470
- Tegmark, M., et al. 2004a, *ApJ*, 606, 702
- Tegmark, M., et al. 2004b, *Phys. Rev. D*, 69, 103501
- Totsuji, H., & Kihara, T. 1969, *PASJ*, 21, 221
- Verde, L., et al. 2002, *MNRAS*, 335, 432
- Watts, P., & Coles, P. 2003, *MNRAS*, 338, 806
- White, S. D. M. 1979, *MNRAS*, 186, 145
- Yahata, K., et al. 2005, *PASJ*, 57, 529
- York, D. G., et al. 2000, *AJ*, 120, 1579.
- Zehavi, I., et al. 2002, *ApJ*, 571, 172
- Zehavi, I., et al. 2005, *ApJ*, in press (astro-ph/0408569)